Electronic Supplementary Material (ESI) for Sustainable Energy & Fuels.

Supporting Information:

Enhanced alkaline hydrogen evolution performance of ruthenium by synergistic doping of cobalt and phosphorus

Chun Hu,[a,c] Wei Zhao,[a] Fuqiang Huang,*[a,b] and Jiacheng Wang,*[a,b]

[a] State Key Laboratory of High Performance Ceramics and Superfine Microstructure, Shanghai Institute of Ceramics, Chinese Academy of Sciences, Shanghai 200050, China

[b] Center of Materials Science and Optoelectronics Engineering, University of Chinese Academy of Sciences, Beijing 100049, China

[c] University of the Chinese Academy of Sciences, Beijing 100049, China

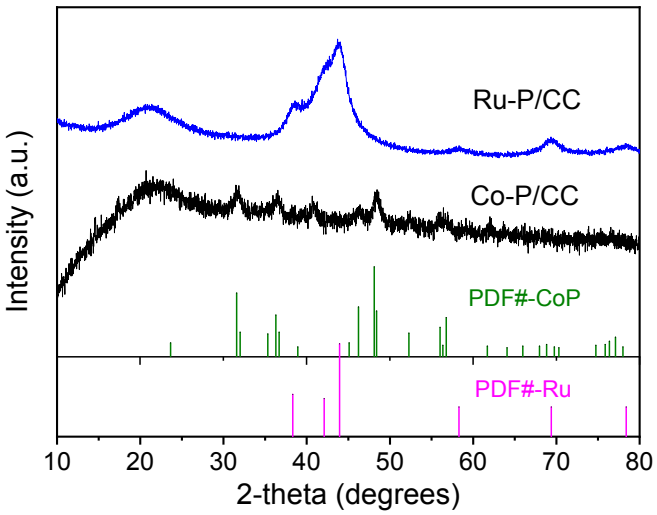

Fig. S1 XRD patterns of Ru-P/CC and Co-P/CC.

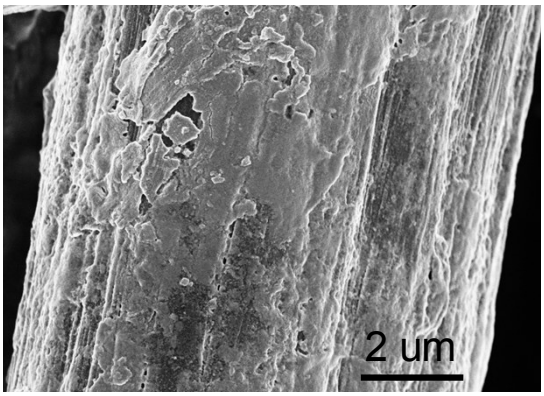

Fig. S2 Low-magnification SEM image for RuCo-P/CC.

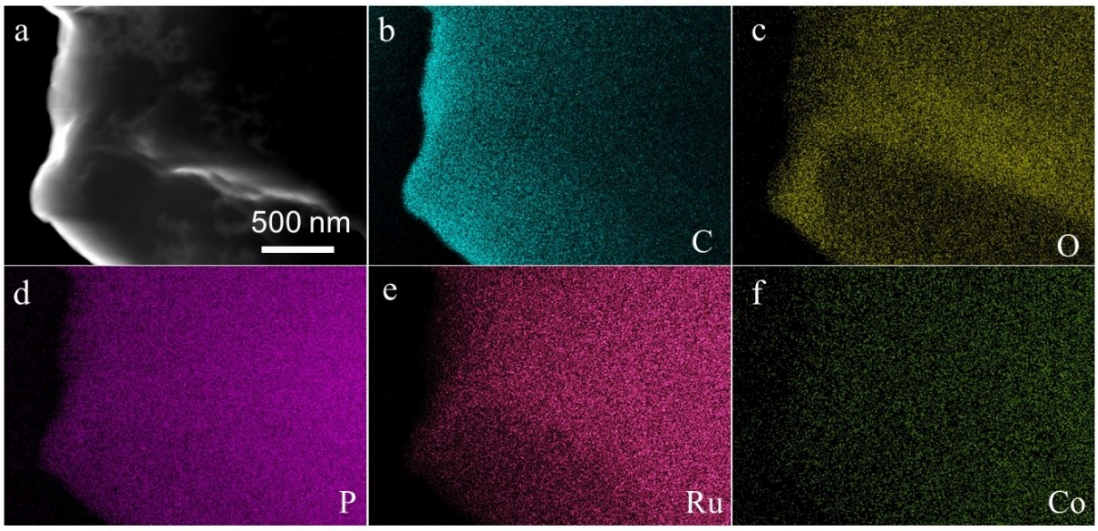

Fig. S3 The corresponding SEM EDS mappings for RuCo-P show the homogeneously distributed of C (b), O (c), P (d), Ru (e) and Co (f) elements.

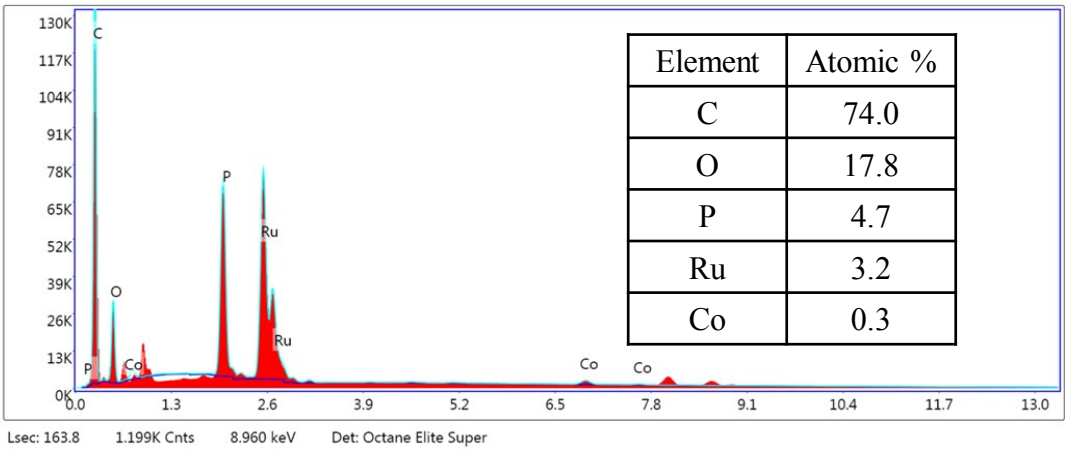

Element	Atomic %
C	74.0
O	17.8
P	4.7
Ru	3.2
Co	0.3

Fig. S4 SEM EDS spectrum of RuCo-P/CC (Inset is the atomic content for Ru, Co, P, O and C elements).

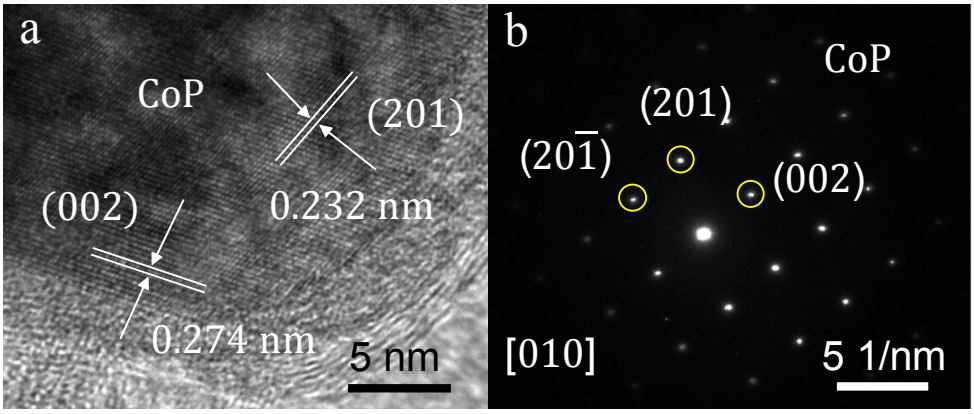

Fig. S5 HRTEM image (a) and corresponding SAED (b) of Co-P/CC.

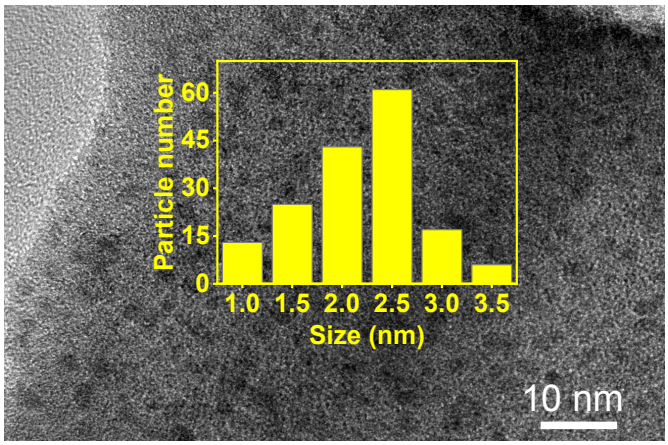

Fig. S6 HRTEM image of Ru-P/CC (inset is the particle size distribution).

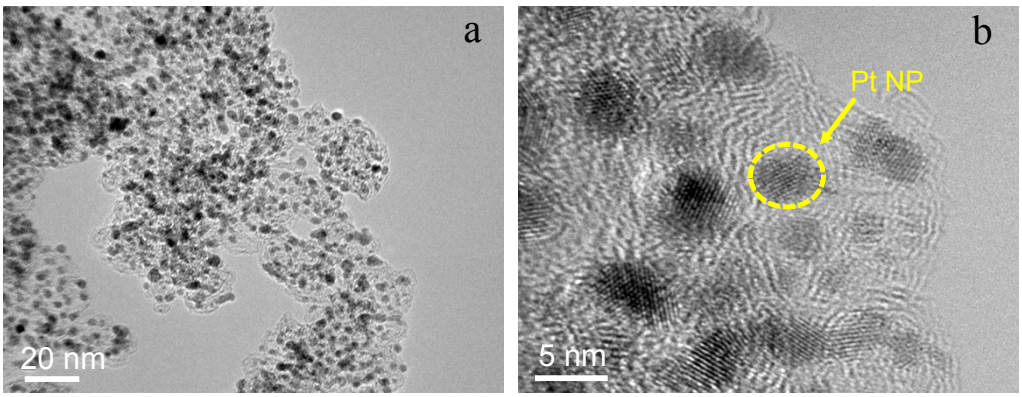

Fig. S7 TEM (a) and HRTEM images of commercial Pt/C.

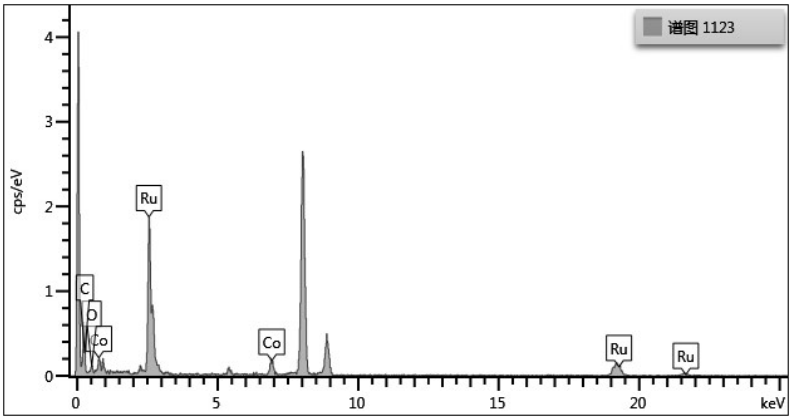

Element	Wt.%	At.%
C	5.32	29.31
O	1.84	7.59
Co	4.97	5.57
Ru	87.88	57.52
Total	100	100

Fig. S8 TEM energy dispersive X-ray spectroscopy (TEM-EDS) results of RuCo/CC.

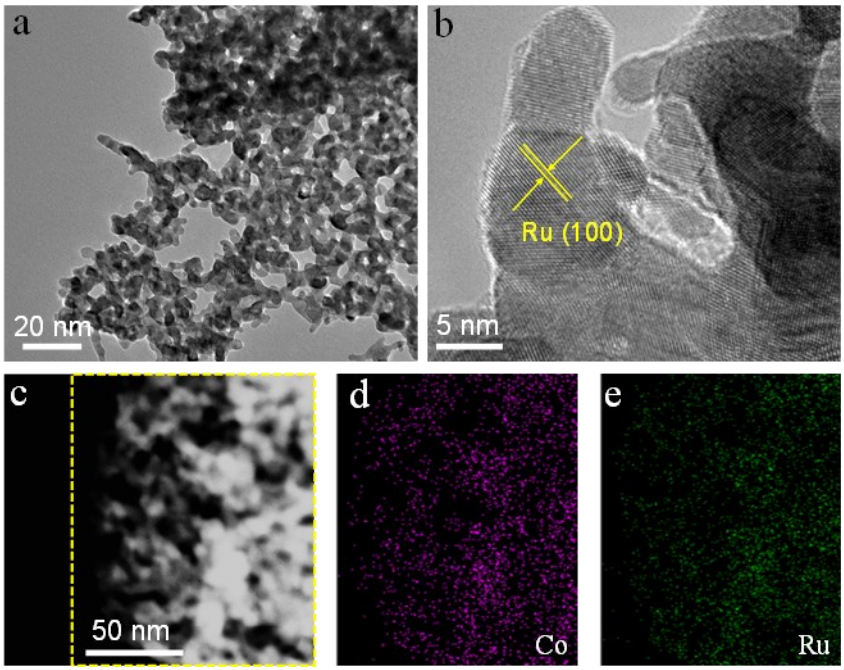

Fig. S9 (a) TEM, (b) HRTEM, (c) HAADF-STEM images, and corresponding elemental mapping of Co (d) and Ru (e) of RuCo/CC.

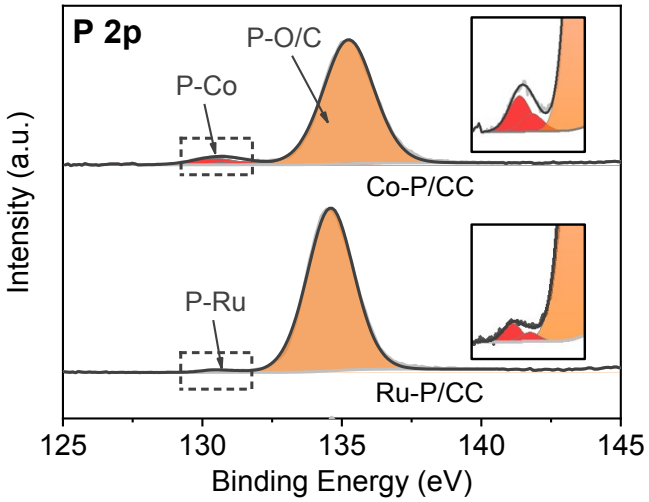

Fig. S10 P 2p XPS spectrum of Co-P/CC and Ru-P/CC.

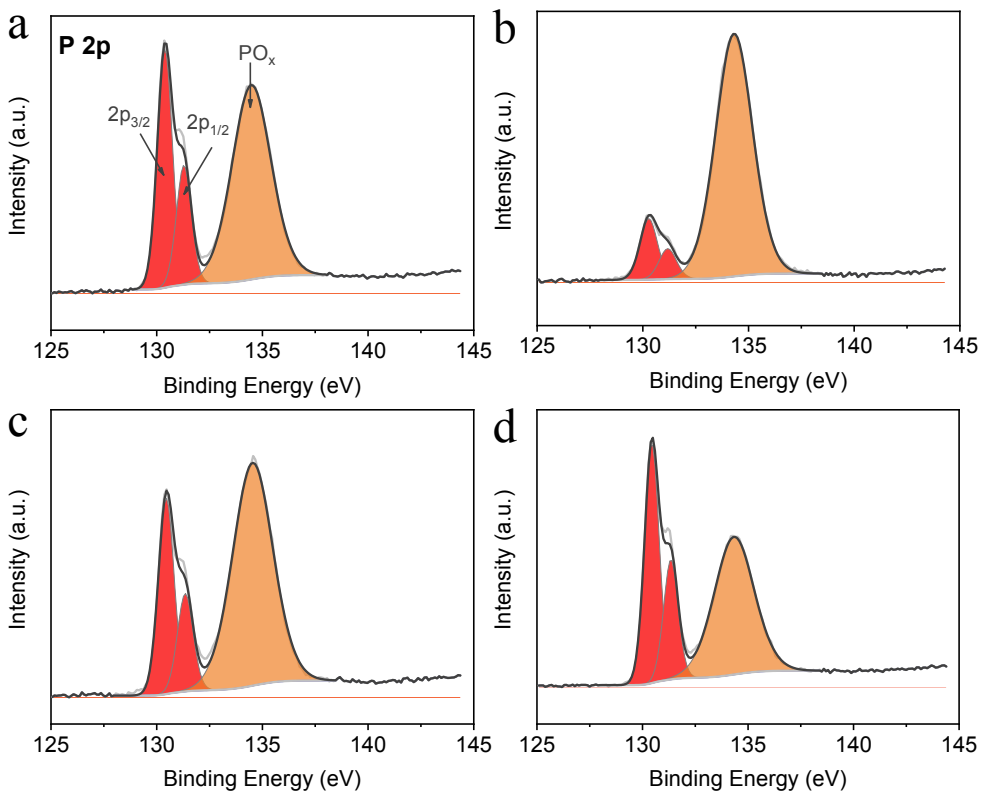

Fig. S11 P 2p XPS spectrum of RuCo-P(1-9)/CC (a), RuCo-P(3-7)/CC (b), RuCo-P(5-5)/CC (c) and RuCo-P(7-3)/CC (d).

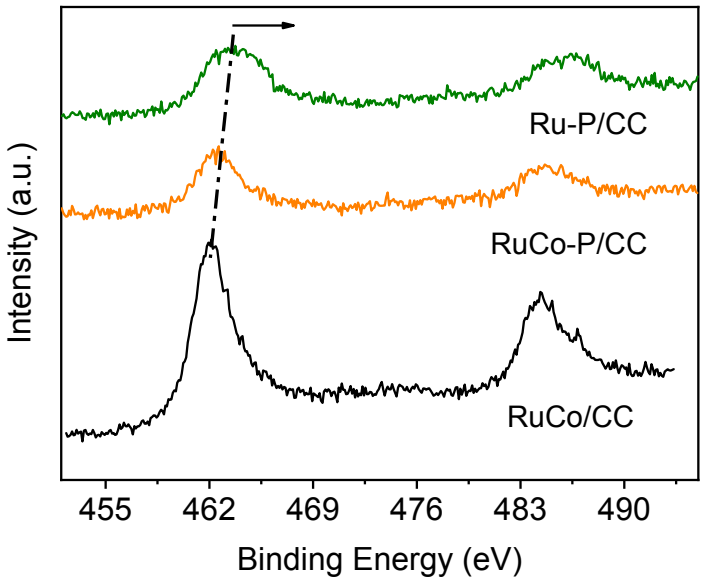

Fig. S12 Ru 3p XPS spectrum of of Ru-P/CC, RuCo/CC and RuCo-P/CC.

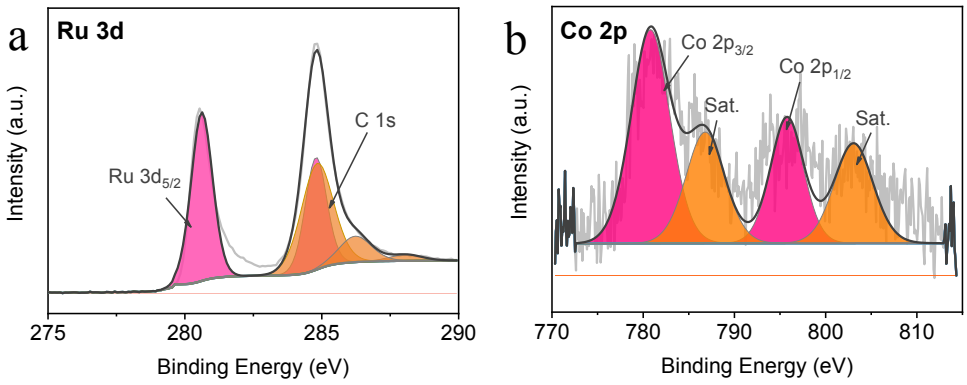

Fig. S13 (a) Ru 3d and (b) Co 2p XPS spectrum of RuCo/CC.

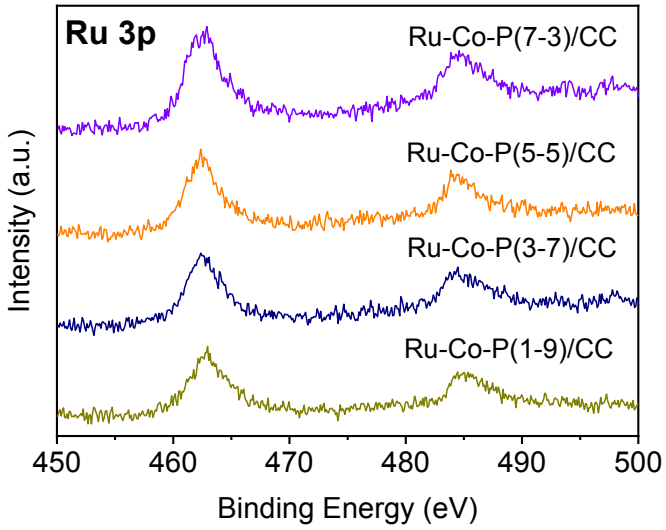

Fig. S14 Ru 3p XPS spectrum of RuCo-P(1-9)/CC, RuCo-P(3-7)/CC, RuCo-P(5-5)/CC and RuCo-P(7-3)/CC.

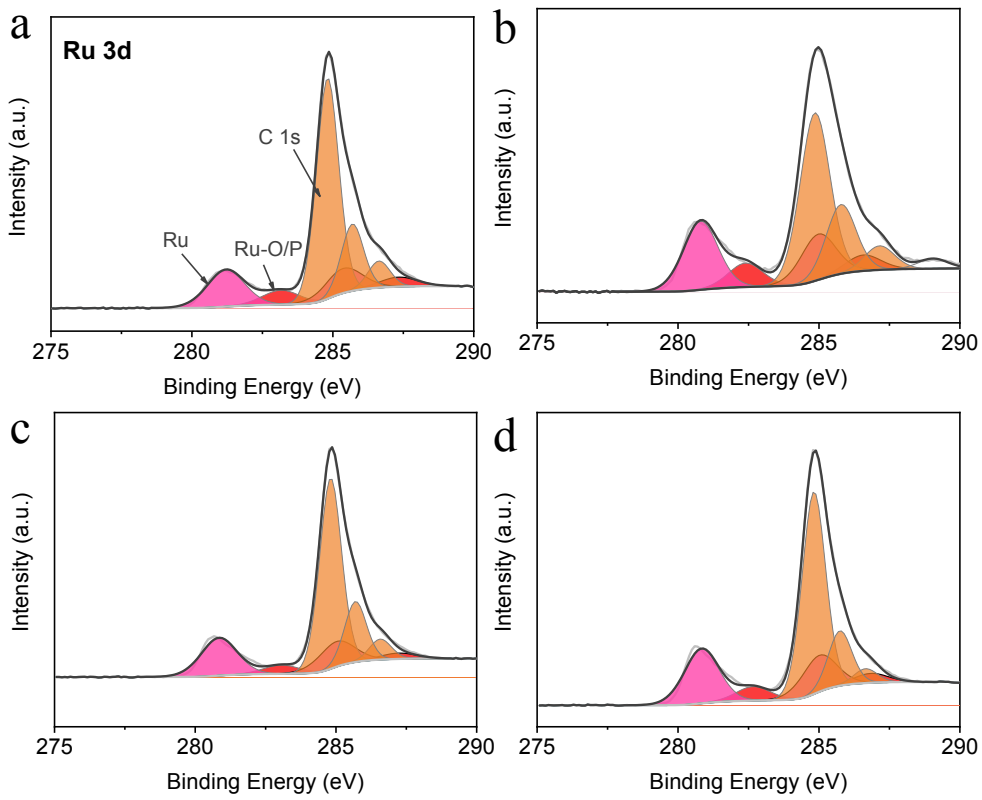

Fig. S15 Ru 3d XPS spectrum of RuCo-P(1-9)/CC (a), RuCo-P(3-7)/CC (b), RuCo-P(5-5)/CC (c) and RuCo-P(7-3)/CC (d).

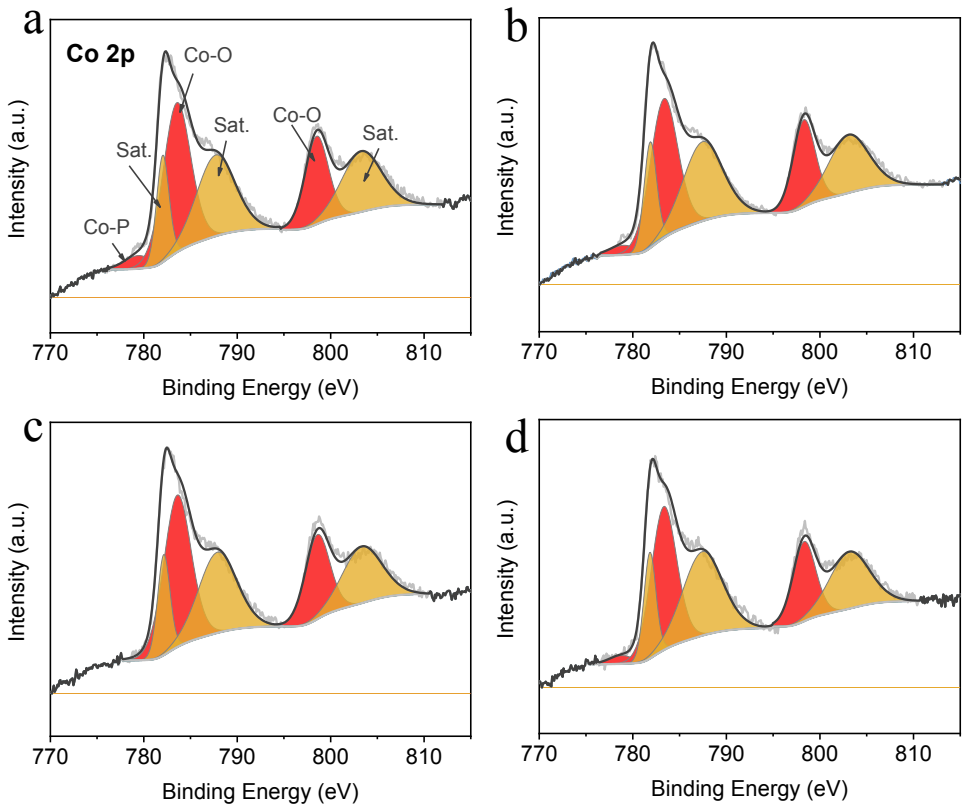

Fig. S16 Co 2p XPS spectrum of RuCo-P(1-9)/CC (a), RuCo-P(3-7)/CC (b), RuCo-P(5-5)/CC (c) and RuCo-P(7-3)/CC (d).

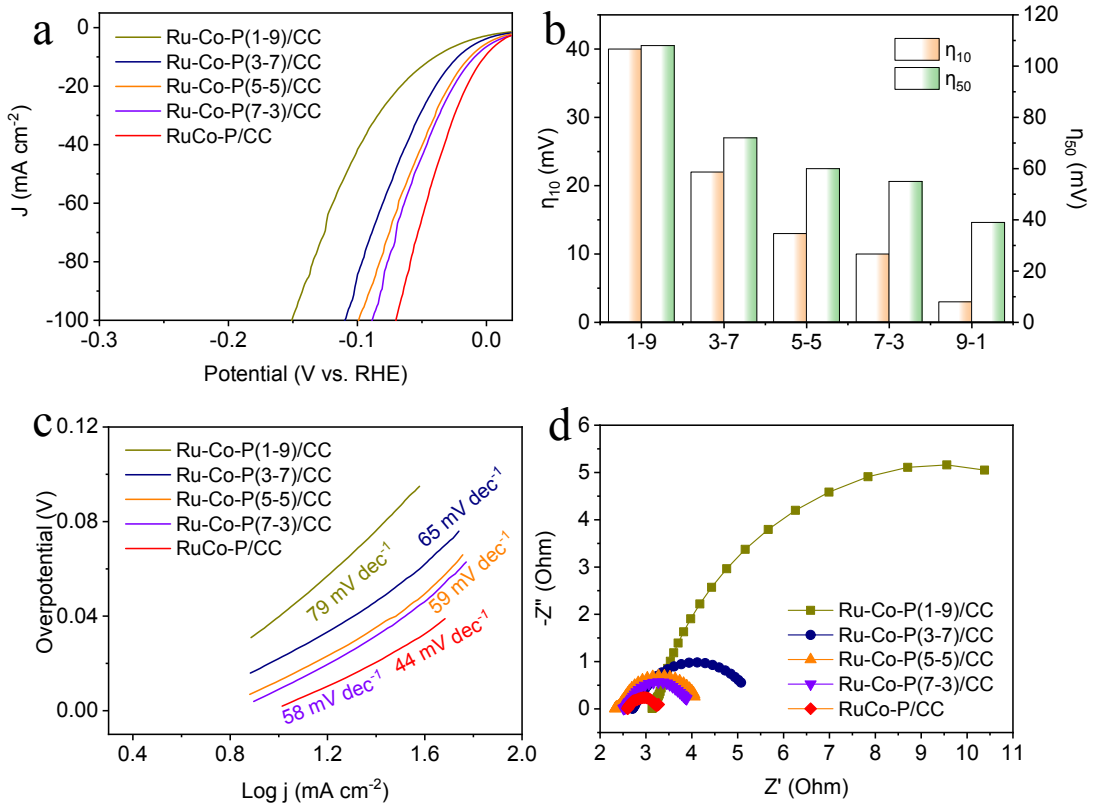

Fig. S17 (a) Polarization curves (iR-corrected) of RuCo-P(1-9)/CC, RuCo-P(3-7)/CC, RuCo-P(5-5)/CC, RuCo-P(7-3)/CC and RuCo-P /CC in 1M KOH electrolyte, scan rate: 2 mV s^{-1}; (b) The overpotential to achieve a current density of 10 mA cm^{-2} (η_{10}) and 50 mA cm^{-2} (η_{50}) of RuCo-P(1-9)/CC, RuCo-P(3-7)/CC, RuCo-P(5-5)/CC, RuCo-P(7-3)/CC and RuCo-P /CC; (c) The corresponding Tafel plots of RuCo-P(1-9)/CC, RuCo-P(3-7)/CC, RuCo-P(5-5)/CC, RuCo-P(7-3)/CC and RuCo-P /CC; (d) Nyquist plots of RuCo-P(1-9)/CC, RuCo-P(3-7)/CC, RuCo-P(5-5)/CC, RuCo-P(7-3)/CC and RuCo-P /CC.

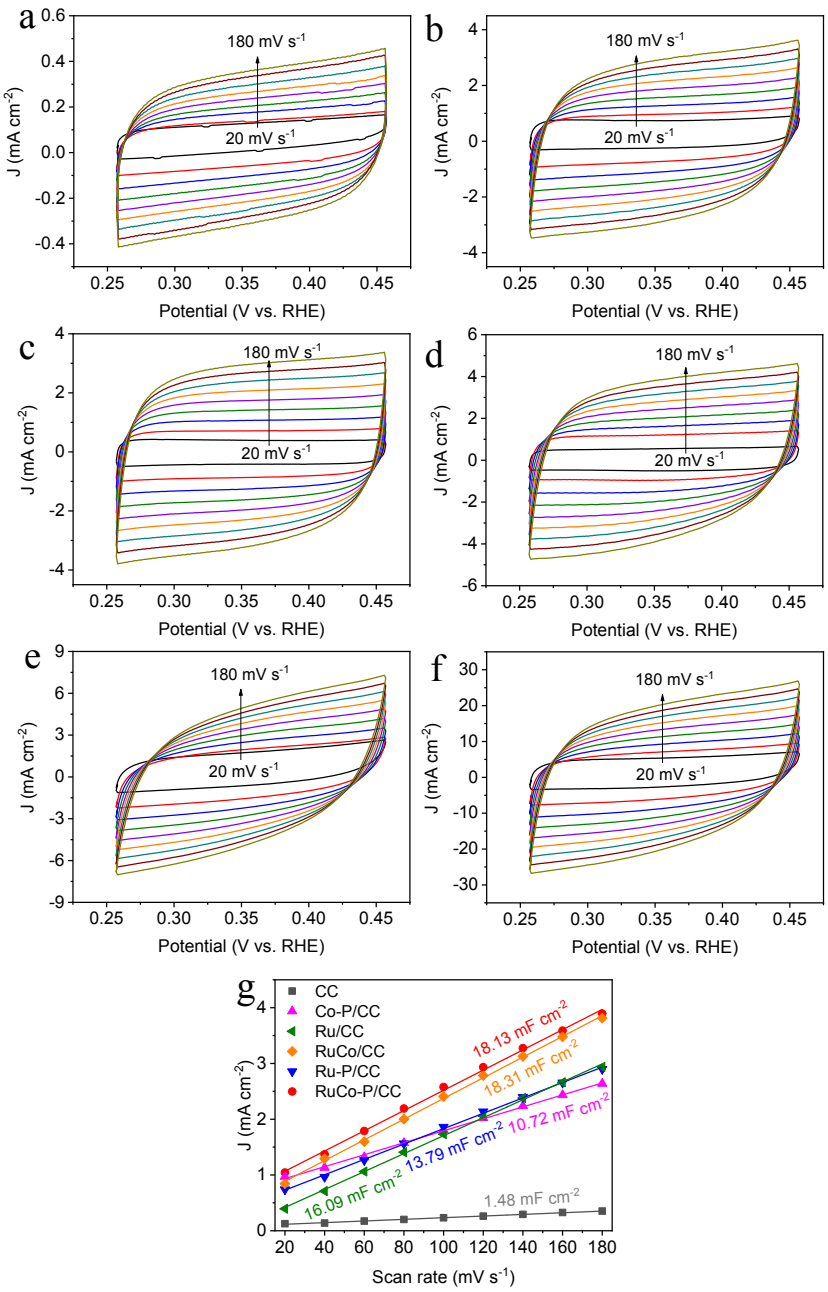

Fig. S18 Cyclic Voltammetry curves with various scan rate (from 20 mV s^{-1} to 180 mV s^{-1}) for CC (a), Co-P/CC (b), Ru/CC (c), RuCo-P/CC (d), Ru-P/CC (e) and RuCo-P/CC (f); (g) the electrochemical double layer capacitance (C_{dl}) of CC, Co-P/CC, Ru/CC, RuCo/CC, Ru-P/CC, RuCo-P/CC.

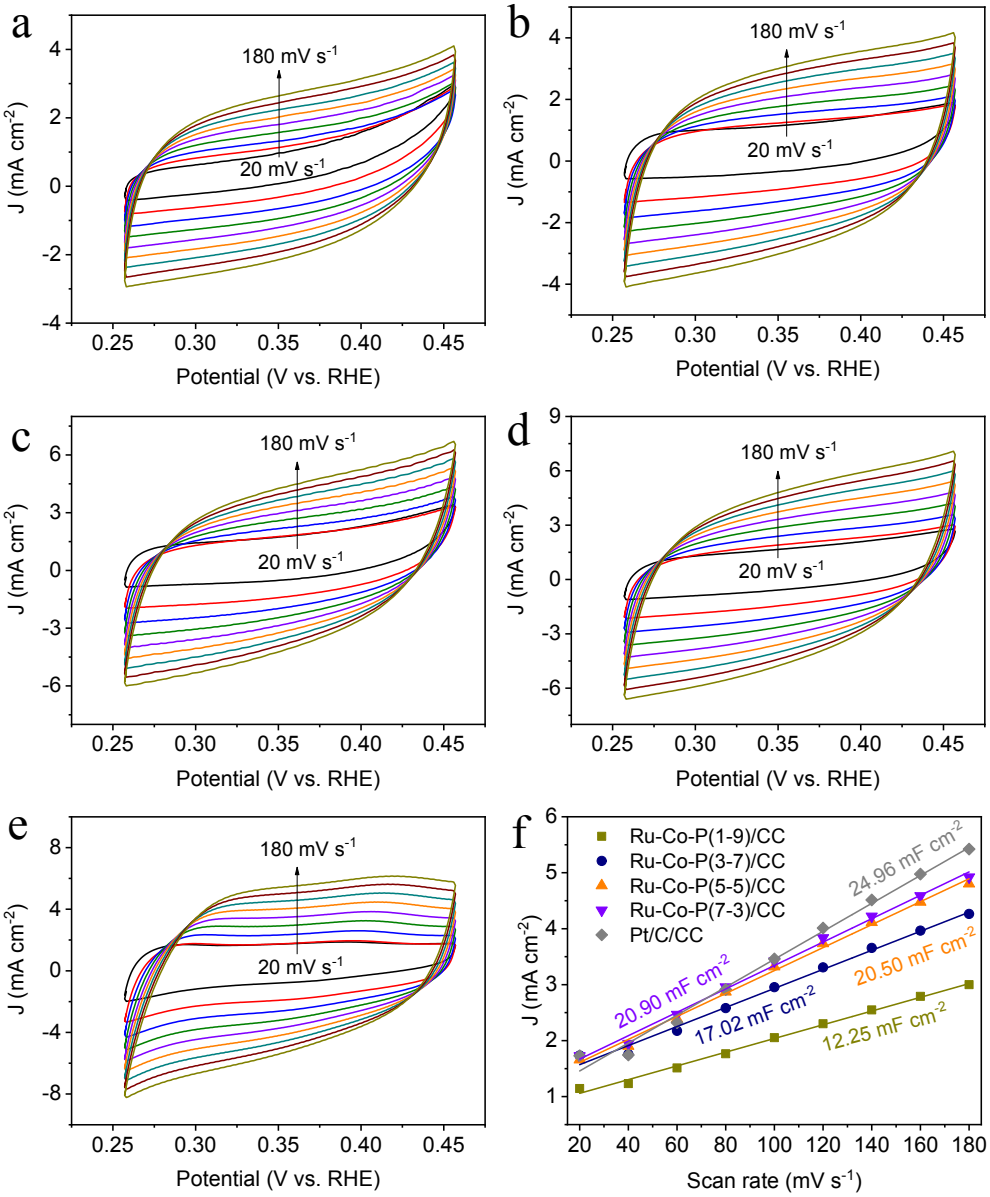

Fig. S19 Cyclic Voltammetry curves with various scan rate (from 20 mV s^{-1} to 180 mV s^{-1}) for RuCo-P(1-9)/CC (a), RuCo-P(3-7)/CC (b), RuCo-P(5-5)/CC (c), RuCo-P(7-3)/CC (d) and Pt/C/CC (e); (f) the electrochemical double layer capacitance (C_{dl}) of RuCo-P(1-9)/CC, RuCo-P(3-7)/CC, RuCo-P(5-5)/CC, RuCo-P(7-3)/CC and Pt/C/CC.

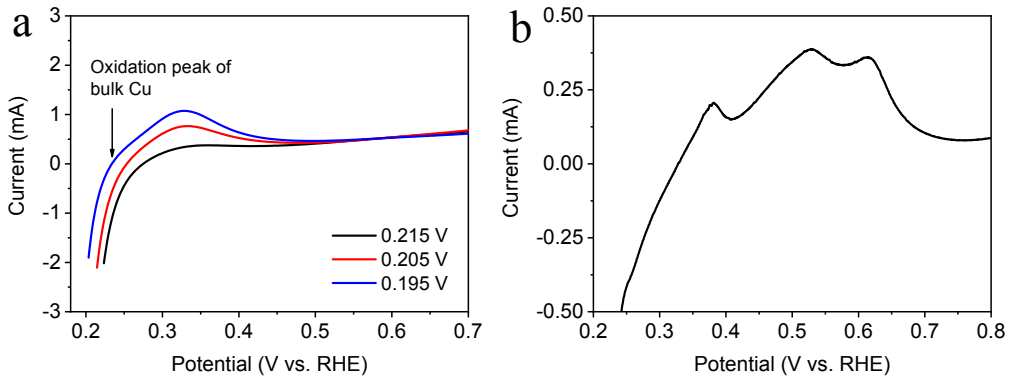

Fig. S20 (a) Cu UPD in 0.5 M H_2SO_4 in the presence of 5 mM $CuSO_4$ on RuCo-P/CC. The electrode was polarized at 0.215, 0.205, and 0.195 V for 100 s to form the UPD layers, respectively. (b) Cu UPD in 0.5 M H_2SO_4 in the presence of 5 mM $CuSO_4$ on Pt/C/CC. The electrode was polarized at 0.205 V.

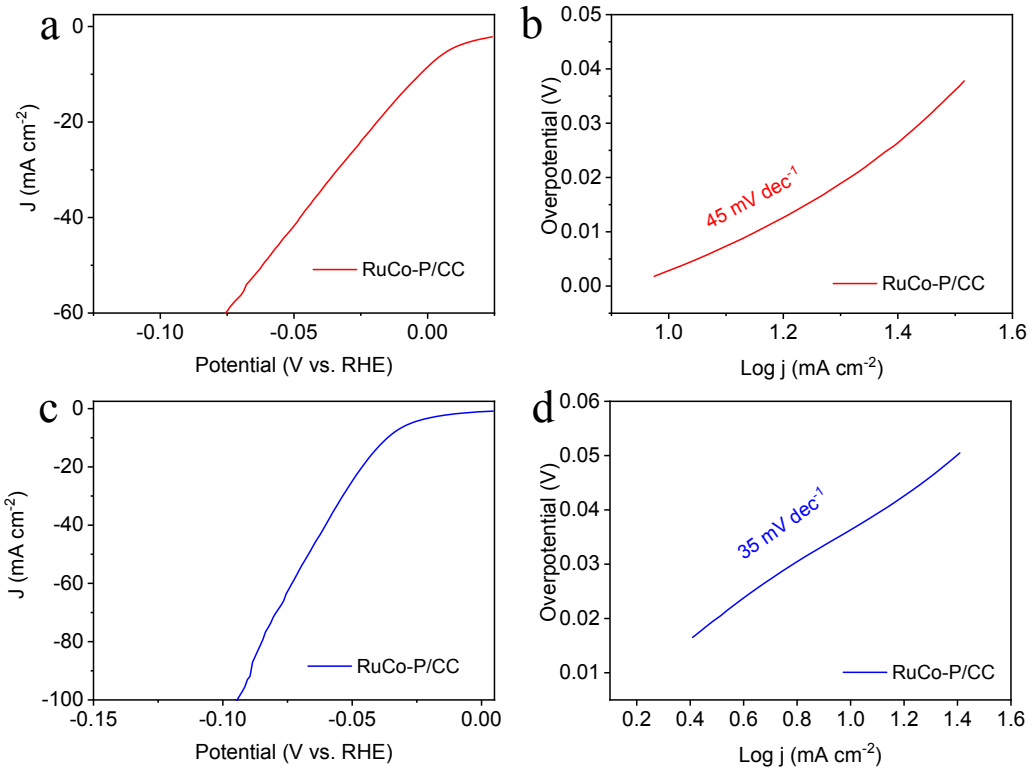

Fig. S21 (a) Polarization curves (iR-corrected) and (b) Tafel slope of RuCo-P/CC in 1M PBS solution. (c) Polarization curves (iR-corrected) and (d) Tafel slope of RuCo-P/CC in 0.5 M H_2SO_4 solution.

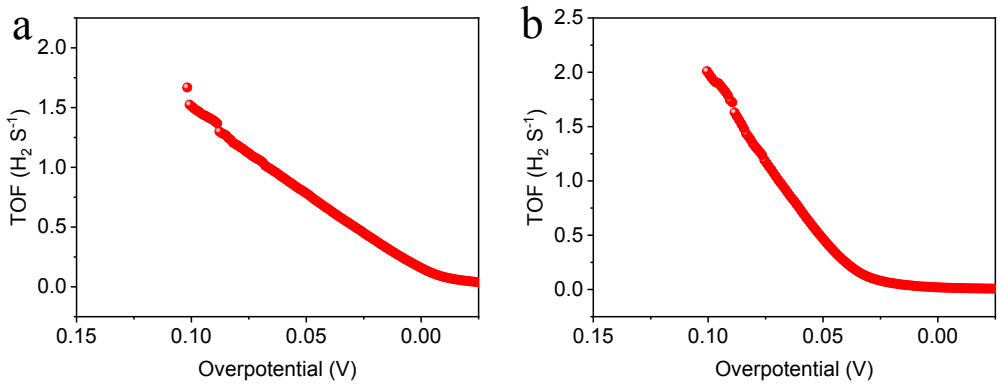

Fig. S22 Turnover frequency (TOF) value of RuCo-P/CC in 1M PBS (a) and 0.5M H_2SO_4 (b).

Table S1 Summary of recently reported HER electrocatalysts grown on carbon cloth in alkaline electrolytes.

Catalyst	Electrolyte	Overpotential at 10 mA cm^{-2} (mV)	Tafel slope ($mV\ dec^{-1}$)
RuCo-P/CC (this work)	1M KOH	4	43
CDs/Pt-PANI/CC[1]	1M KOH	56	58
N-Co-P/CC[2]	1M KOH	39	51
W-CoP NAs/CC[3]	1M KOH	94	63
VN@Ni_3N–Ni/CC[4]	1M KOH	57	40
$Mo_{0.25}Co_{0.75}P$/CC[5]	1M KOH	59	52
Ru–TA/ACC[6]	1M KOH	29	35
Co_3S_4/EC-MOF/CC[7]	1M KOH	84	82
Co@N-CS/N-HCP@CC[8]	1M KOH	66	65
N–Co_2P/CC[9]	1M KOH	39	58
N-$NiMoO_4$/NiS_2/CC[10]	1M KOH	99	74.2
Ni-FeP/TiN/CC[11]	1M KOH	75	73
Pt-CoS_2/CC[12]	1M KOH	24	82

Table S2 Comparison of the turnover frequency (TOF) value of recently reported HER electrocatalysts grown on three dimensional substrates (carbon cloth/carbon paper/Ni foam/Ti plate).

Catalyst	Electrolyte	TOF (H_2 s^{-1})
RuCo-P/CC	1M KOH	1.31 at η=50 mV; 3.03 at η=100 mV
	1M PBS	0.81 at η=50 mV
	0.5M H_2SO_4	0.58 at η=50 mV; 2.01 at η=100 mV
Pt/C/CC	1M KOH	0.96 at η=50 mV; 2.48 at η=100 mV
VN@Ni_3N–Ni/CC[4]	1M KOH	0.176 at η=100 mV
$Ni_{0.1}Co_{0.9}P$/CP[13]	1M PBS	0.24 at η=125 mV
CoP/Ni_5P_4/CoP/Ni foam[14]	0.5 M H_2SO_4	0.453 at η=75 mV; 1.22 at η=100 mV
Ru–TA/ACC[6]	1M KOH	0.48 at η=25 mV; 1.05 at η=50 mV
CC@N-CoP[15]	0.5 M H_2SO_4	0.0199 at η=50 mV
$Cu_{0.075}Co_{0.925}P$/CP[16]	0.5 M H_2SO_4	0.15 at η=100 mV
Ce doped CoP/ Ti plate[17]	0.5 M H_2SO_4	0.36 at η=100 mV

References for supporting information:

1. Q. Dang, Y. Sun, X. Wang, W. Zhu, Y. Chen, F. Liao, H. Huang and M. Shao, *Appl. Catal. B*, 2019, **257**, 117905.
2. Y. Men, P. Li, J. Zhou, G. Cheng, S. Chen and W. Luo, *ACS Catal.*, 2019, **9**, 3744-3752.
3. X. Wang, Y. Chen, B. Yu, Z. Wang, H. Wang, B. Sun, W. Li, D. Yang and W. Zhang, *Small*, 2019, **15**, e1902613.
4. X. Dong, H. Yan, Y. Jiao, D. Guo, A. Wu, G. Yang, X. Shi, C. Tian and H. Fu, *J. Mater. Chem. A*, 2019, **7**, 15823-15830.
5. Y. Zhang, Z. Wang, F. Du, H. He, A. Alsaedi, T. Hayat, T. Li, G.-L. Li, Y. Zhou and Z. Zou, *J. Mater. Chem. A*, 2019, **7**, 14842-14848.
6. J. Chen, H. Wang, Y. Gong and Y. Wang, *J. Mater. Chem. A*, 2019, **7**, 11038-11043.
7. T. Liu, P. Li, N. Yao, T. Kong, G. Cheng, S. Chen and W. Luo, *Adv. Mater.*, 2019, **31**, e1806672.
8. Z. Chen, Y. Ha, H. Jia, X. Yan, M. Chen, M. Liu and R. Wu, *Adv. Energy Mater.*, 2019, **9**, 1803918.
9. Y. Men, P. Li, F. Yang, G. Cheng, S. Chen and W. Luo, *Appl. Catal. B*, 2019, **253**, 21-27.
10. L. An, J. Feng, Y. Zhang, R. Wang, H. Liu, G.-C. Wang, F. Cheng and P. Xi, *Adv. Funct. Mater.*, 2019, **29**, 1805298.
11. X. Peng, A. M. Qasim, W. Jin, L. Wang, L. Hu, Y. Miao, W. Li, Y. Li, Z. Liu, K. Huo, K.-y. Wong and P. K. Chu, *Nano Energy*, 2018, **53**, 66-73.
12. X. Han, X. Wu, Y. Deng, J. Liu, J. Lu, C. Zhong and W. Hu, *Adv. Energy Mater.*, 2018, **8**, 1800935.
13. R. Wu, B. Xiao, Q. Gao, Y. R. Zheng, X. S. Zheng, J. F. Zhu, M. R. Gao and S. H. Yu, *Angew. Chem. Int. Ed.*, 2018, **57**, 15445-15449.
14. I. K. Mishra, H. Zhou, J. Sun, F. Qin, K. Dahal, J. Bao, S. Chen and Z. Ren, *Energy Environ. Sci.*, 2018, **11**, 2246-2252.
15. Q. Zhou, Z. Shen, C. Zhu, J. Li, Z. Ding, P. Wang, F. Pan, Z. Zhang, H. Ma, S. Wang and H. Zhang, *Adv. Mater.*, 2018, **30**, e1800140.
16. L. Yan, B. Zhang, J. Zhu, S. Zhao, Y. Li, B. Zhang, J. Jiang, X. Ji, H. Zhang and P. K. Shen, *J. Mater. Chem. A*, 2019, **7**, 14271-14279.
17. W. Gao, M. Yan, H.-Y. Cheung, Z. Xia, X. Zhou, Y. Qin, C.-Y. Wong, J. C. Ho, C.-R. Chang and Y. Qu, *Nano Energy*, 2017, **38**, 290-296.